Influence of Geometry on Failure Modes of Hybrid Metal-Composite Protruding Bolted Joints

Calin-Dumitru COMAN*

*Corresponding author
INCAS – National Institute for Aerospace Research "Elie Carafoli",
B-dul Iuliu Maniu 220, Bucharest 061126, Romania,
coman.calin@incas.ro

DOI: 10.13111/2066-8201.2021.13.3.3

Received: 15 March 2021/ Accepted: 28 June 2021/ Published: September 2021

Abstract: *This article presents the influence of joint geometry on the damage mode in the CFRP (Carbon Fiber Reinforced Polymer) composite plate of the single-lap, protruding, hybrid metal-composite joints. A detailed 3D finite element model incorporating geometric, material and friction-based contact full nonlinearities is developed to numerically investigate the geometry effects on the progressive damage analysis (PDA) of the orthotropic material model. The PDA material model integrates the nonlinear shear response, Hashin-tape failure criteria and strain-based continuum degradation rules being developed using the UMAT user subroutine in Nastran commercial software. In order to validate the geometry effects on the failure modes of the joints with hexagonal head bolts, experiments were conducted using the SHM (Structural Health Monitoring) technique. The results showed that the plate geometry is an important parameter in the design process of an adequate bolted joint and its effects on damage initiation and failure modes were quite accurately predicted by the PDA material model, which proved to be computational efficient and can predict failure propagation and damage mechanism in hybrid metal-composite bolted joints.*

Key Words: *Hybrid bolted joints, progressive damage analysis, finite element analysis, geometry, failure modes*

1. INTRODUCTION

The aerospace industry became the most common application field for fiber-reinforced polymer matrix composites (PMCs) due to their lightweight properties [1]. These structural components are often assembled in conjunction with metal parts using mechanically fastened joints resulting in hybrid metal-composite joints. Up to nowadays, the researchers studied the failure analysis of composite bolted joints using a method that combines continuum damage mechanics (CDM) [2] with finite element analysis (FEA). The major disadvantage of the CDM models is the huge amount of test data required for model calibration. The progressive damage analysis (PDA) in composite materials, which is based on the stress-strain failure criterion, showed that the material orthotropic properties reduction due to damage initiation is essential for the stress field analysis [3-7]. A lot of PDA models in the research field [8-11] have incorporated shear nonlinearity, Hashin-type failure criterion, and constant degradation of low elastic properties for orthotropic materials, which makes the method quite easy to implement and computationally efficient. A lot of research PDA models [8-11] incorporated shear nonlinearity. Because these properties degradation models used constant factors to reduce elastic properties due to the increased damage, the models could not predict the final bearing

failure. Models containing continuous degradation rules started to appear in the literature [12], [13] to improve the numeric algorithm converge and to obtain a smoother loading-displacement curve. The composite progressive damage behavior is a complex nonlinear phenomenon and, in conjunction with geometric and contact nonlinearities, can lead to divergence of the finite element method (FEM) analysis, [14]. The difficulties arising from composite materials usage on structural failure problems are that these materials have anisotropic mechanical properties, brittle and low inter-laminar strength [15]. Awadhani et al. [16] presented a numerical and experimental study for the influence of a geometry parameter (edge distance to bolt diameter ratio, *e/d*) onto the stiffness, strength and failure modes of a hybrid metal-GFRP (Glass Fibers Reinforced Plastic) single-lap, single-bolt joints with steel bolts. The conclusions of the study were that the *e/d* ratio varied the failure modes from cleavage to bearing mode. It was also observed that the geometric parameter has increased the joint tensile strength and also increased the yield load. In this study it is described and developed a progressive damage analysis using an adequate material model for composite plate that can predict the geometry parameters (width to bolt diameter -*w/d*-) effects on structural behavior and failure modes of hybrid metal-composite bolted joints. The analysis takes into account all the nonlinearities phenomena involved in load transition through the joint as geometric nonlinearity, friction-based contact, and material nonlinearities due to shear deformations of the lamina. Hashin-type failure criterion and strain-based continuous degradation rules were implemented using a user subroutine coded in Fortran programming language and commercial Nastran SOL 400 solver. A series of experiments were conducted in order to validate the FE model and PDA results, involving the influence of temperature on the failure modes of the hybrid-metal composite joints. The experimental and numerical results fit quite accurately for the influence of geometry parameters (*w/d*, *e/d*) and failure load of hybrid metal-composite, bolted joints.

2. PROBLEM DESCRIPTION

- Joint geometry description

Single-lap joints (SLJ) with protruding hexagonal head bolt were manufactured using both metal and composite materials for the adherents. The joint geometry was chosen in accordance with ASTM standard [17] to induce bearing failure. The in-plane dimensions of the plates are presented in Table 1 and Fig.1. The metal plate thickness is 4 mm and 3 mm for the composite one. Hexagonal head stainless steel bolts with 5 mm nominal diameter were used. The applied torque level for bolt was 0.5 N m. The composite plate was made of carbon-epoxy pre-pregs with fiber volume fraction of 32%. The stacking sequence is defined by [0/90/0/90/0/90] using 0.33 mm thickness unidirectional lamina, with the elastic properties presented in Table 2. The metal plate was manufactured from aluminum alloy AA 7075T6 [18] and the bolts, nuts and washers were made of stainless steel A2-70 [18] with the elastic properties shown in Table 2, as well. A lot of five specimens for each case presented in Table 1 were prepared for the geometry influence on the failure modes in the laminated plate. The experimental models are presented in Fig. 2.

Table1. Experiment set-up

Geometry case	Nb. of specimens	Length (mm)	Width (mm)	Torque (Nm)
1	5	150	34	0.5
2		150	42	
3		150	50	

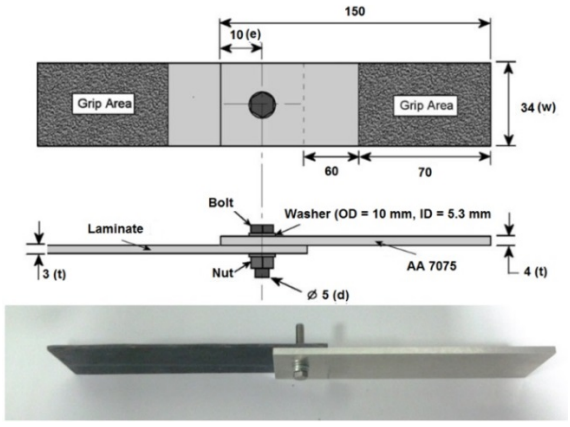

Fig. 1 Joint geometry, geometry case 1

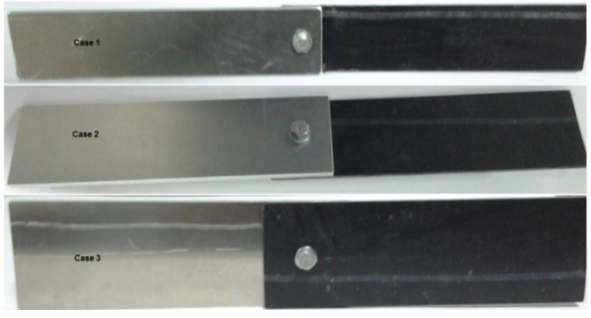

Fig. 2 Experimental models, geometry cases

Table 2. Mechanical properties of the materials

Property	CFRP Lamina	AA 7075T6 Ref. [18]	A2-70 Ref. [18]
Longitudinal modulus E_{11} (MPa)	34433	71016	206000
Transversal modulus E_{22} (MPa)	3610		
Through-thickness modulus, E_{33} (MPa)	3610		
Shear modulus G_{12} (MPa)	2421	26890	75842
Shear modulus G_{23} (MPa)	2421		
Shear modulus G_{13} (MPa)	1561		
Poisson coefficient υ_{12}	0.36	0.33	0.36
Poisson coefficient υ_{23}	0.45		
Poisson coefficient υ_{13}	0.35		
Longitudinal tensile strength $\sigma_{11,\,max}^{T}$, (MPa)	253		
Longitudinal compression strength $\sigma_{11,\,max}^{C}$, (MPa)	230		
Transversal compression strength $\sigma_{22,\,max}^{C}$, (MPa)	74		
In plane shear strength τ_{12}^{max}, (MPa)	25		
Out plane shear strength τ_{23}^{max}, (MPa)	37		
Out plane shear strength τ_{13}^{max}, (MPa)	37		

Note: (1, 2, 3) are the lamina on axis coordinate system.

The unidirectional lamina properties presented in Table 2 were obtained using ASTM [19]-[21] standards on the unidirectional laminated coupons. The bearing tests were conducted in accordance with ASTM standard [17]; the specimens were gripped into a 30 kN Instron universal testing machine, the torque level was applied to the bolt and then the displacement controlled tensile loading with 0.3 mm/min was applied until ultimate failure, as it is shown in Fig. 3.

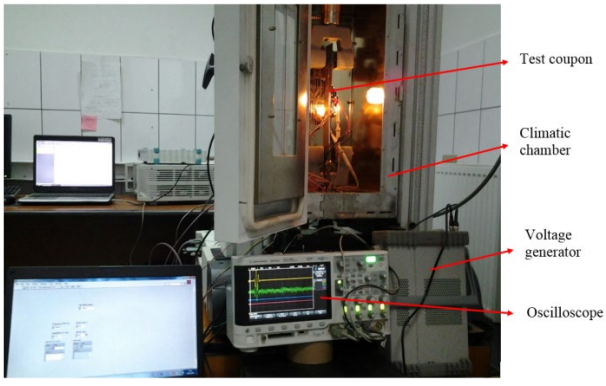

Fig. 3 Experimental workbench

- Numerical analysis

A tridimensional finite element model, with linear brick elements, was developed in commercial software MSC Patran for the joint geometry, as shown in Fig. 4. Each separate part was modeled: metal and composite plates, the washers and a combined bolt-nut part. For simulating the bolt pre-load an axial force (330 N) was applied in the bolt shank using Bolt Preload Module in Patran.

Regarding the clamping of the joint in the test machine, the boundary conditions imposed on the model are presented in Fig.4 and represent the fixing of all translations only on the top and bottom surfaces of the leftmost end of the metal plate and blocking only the translations in y and z directions imposing a prescribed displacement in the *x* direction at the rightmost end of the composite plate.

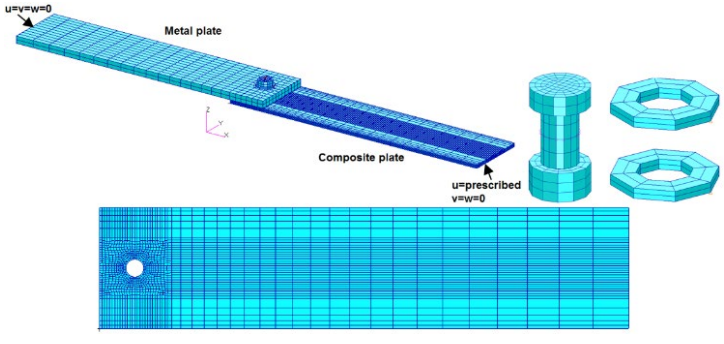

Fig. 4 3D finite element model and boundary conditions

The composite plate is modeled with continuum solid-shell special elements available in MSC Nastran 2012. These special solid elements have bending properties like shells and one integrating point per element. The finite element model has six elements per laminate thickness, with one solid-shell element per each ply, thus, the stress in each ply can be determined and the correct bending-twisting coupling is obtained. All metallic parts are

modeled with continuum solid elements with large strain property assumed. In the 3D model, the contact between all surfaces is achieved by the direct method of constraints. The method requires the definition of contact bodies.

The contact bodies may be the whole physical bodies (laminated plates, bolt, washers), but it has been shown [22] that it is more efficient to consider only the sets of elements of these physical bodies in contact, as shown in Fig. 5, because the number of checks for contact between bodies at each iteration of the solution is more reduced.

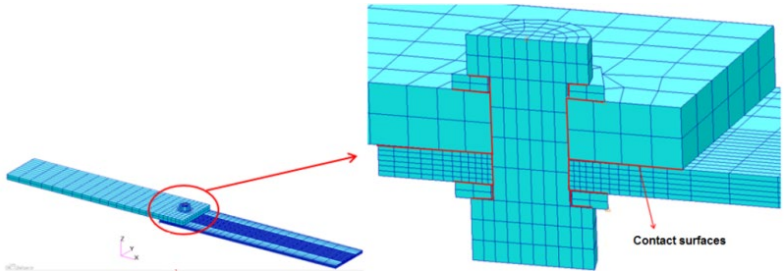

Fig. 5 Contact elements in 3D model

3. GEOMETRY EFFECTS ON THE JOINT FAILURE

- Model validation

In this section, the results from the three-dimensional finite element model are compared with the results of the tests.

Strains at selected points on the surface of the laminated plate are used to check the accuracy of the finite element model.

The joints were strain gauged and loaded in tensile to a level that prevents any damage of the composite plate (1.2 kN) and 0.5 Nm torque level.

Fig. 6 presents the locations of the strain gauges with 3 mm length; all gauges are aligned with the loading direction and are located on the top surface of the laminate plate, except for the gauge number 2 which is located in the shear plane on the bottom surface. The numerical and experimental results for strains are shown in Table 3 and Fig. 7.

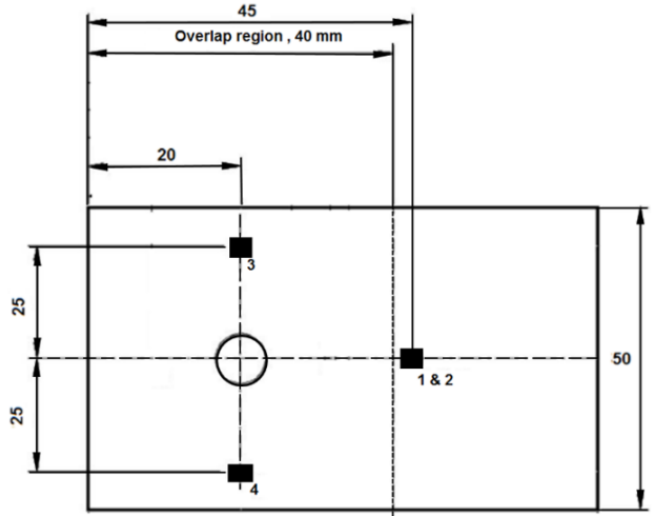

Fig. 6 Strain gauge locations, all dimensions in mm

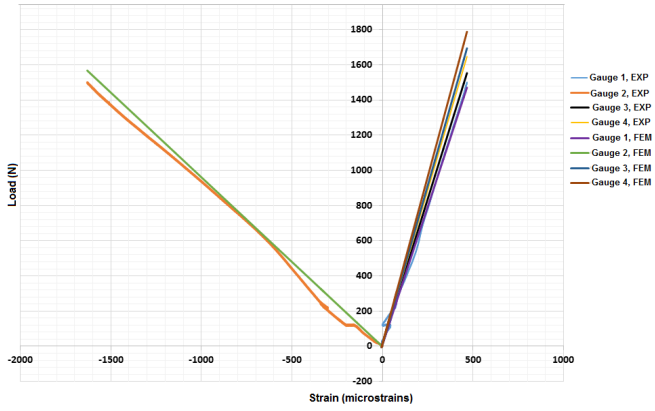

Fig. 7 Experimental and numerical surface strains

Table 3. Experimental and numerical strain gauge results, 1.2 kN load

Gauge number	Experimental strain (μm/m)	Numerical strain (μm/m)
1	376	380
2	-1300	-1252
3	357	329
4	339	315

From Table 3 it was clearly seen that strain gauges 1 and 2 indicate a joint bending, despite the fact that the load is a tensile load. The readings for gauges 3 and 4 are quite different, indicating a twisting effect of the joint along the longitudinal axis which is the loading axis. As a conclusion from the Table 3, it can be considered that the FE model predicted the linear behavior of the joint quite well and it can be used in the following geometry influence study on the failure modes of the hybrid metal-composite joints.

- SHM method description

A common and useful method for structure health monitoring (SHM) is using the guided elastic waves. The major advantage of these waves is the low energy losing while passing through the structure. The pioneer of this method is Horace Lamb [23]. There are two types of propagation modes for these waves: symmetric mode (S_0, S_1…S_n) and anti-symmetric (A_0, A_1…A_n) [24]. The SHM testing technique was used to experimentally observe the first ply failure in the laminate plate. The piezo-electric devices (PWAS) used in this experiment are produced by STEMiNC company, having the part number SMPL7W7T02412. They have a circular shape with 5 mm diameter and are presented in Fig. 8. The company code of the PWAS piezo-electric material is SM412 and the electro-mechanical properties are presented in Table 4, [25]. The input signal is a sinusoidal tone burst type signal having 20 V peak to peak amplitude with Hanning window amplitude modulation. This signal includes 3 periods and is generated by an Agilent 33120 signal generator, see Fig. 9.

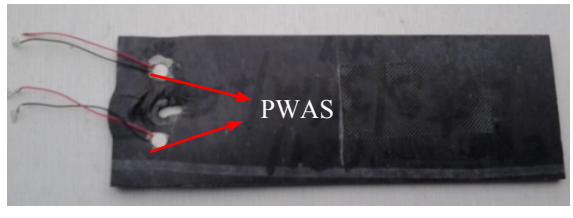

Fig. 8 PWAS positions on composite plate, geometry case 3

Table 4. Electro-mechanical characteristics of the SM412 material, [25]

Property	Symbol	Value	Measurement unit
Electromechanical coupling coefficient	K_p	0.63	
	K_t	0.42	
	K_{31}	0.35	
Frequency constant	N_p	2080	Hz ● m
	N_t	2080	
	N_{31}	1560	
Piezoelectric constant	d_{33}	450	$\times 10^{-12}$m/v
	d_{31}	-190	
	g_{33}	25.6	$\times 10^{-3}$Vm/N
	g_{31}	-12.6	
Elastic Constant	Y_{33}	5.6	$\times 10^{10}$N/m^2
	Y_{11}	7.6	
Mechanical Quality Factor	Q_m	100	
Dielectric Constant	$_{\varepsilon}T_{33/\varepsilon 0}$	1850	@1KHz
Dissipation Factor	tan δ	1.2	%@1KHz
Curie Temperature	T_c	320	°C
Density	r	7.8	g/cm^3

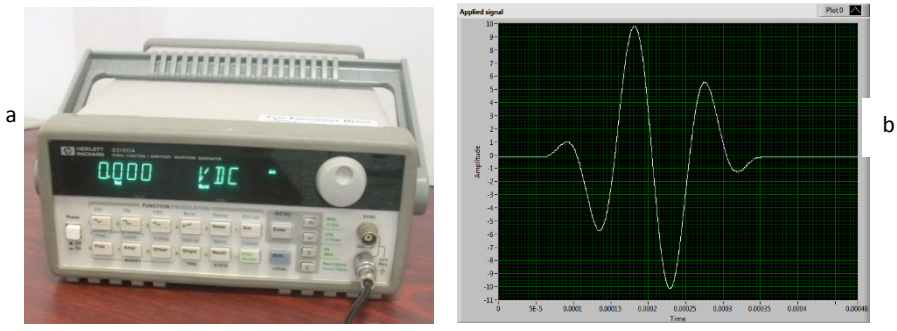

Fig. 9 Hewlett Packard 33120A arbitrary waveform generator

In Fig. 10 it is presented the damage initiation effect on the amplitude of the received signal and force-displacement characteristic curve, in order to be able to identify the first ply failure of the laminated plate.

The amplitude curves represent the maximum (peak to peak) amplitude of each receiving signals during the test.

During a test, the input and output signals of the two PWAS's from the laminated plate are acquired with a period of 2 seconds.

From Fig. 10 it can be clearly seen that the amplitude of the output signal is increasing with the joint stiffening up to the first lamina failure event.

Afterwards, the amplitude is decreasing due to the elastic properties degradation in the

laminate plate on the post failure stage.

As a conclusion, it can be considered that SHM method accurately predicted the first lamina failure and joint limit load which represents the fiber compression damage at the lamina level, because this local damage corresponds to a significant decreasing of the joint stiffness.

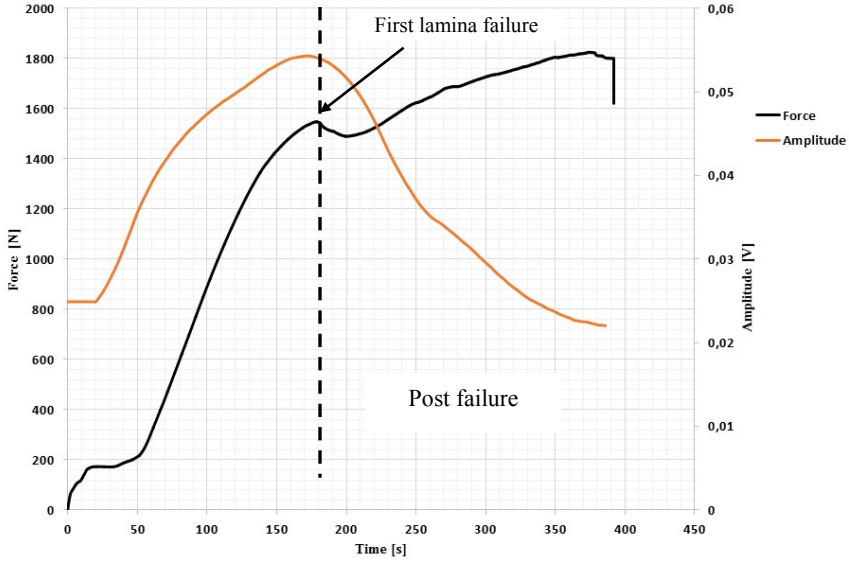

Fig. 10 Damage effects on output signal, geometry case 3

- Nonlinear shear deformation

The simulation must take into account the two most important nonlinear mechanisms: lamina nonlinear shear deformations and stiffness reduction due to damage accumulation at the lamina level.

These two nonlinearities are taken into account using an external user-defined subroutine named USER_MAT, edited in FORTAN language.

USER_MAT calls the modified Nastran material user-defined subroutine UMAT, in order to implement the material nonlinearities specified above.

Hahn and Tsai developed [26] the in-plane nonlinear shear lamina constitutive model using the high-order elasticity theory:

$$\gamma_{12} = \frac{\tau_{12}}{G_{12}} + \beta \cdot \tau_{12}^3 \tag{1}$$

where β is a material parameter that can be determined by experiments only.

Fig. 11 shows the experimental curve of the shear deformation γ_{12} as a function of the shear stress τ_{12} obtained using off-axis tension tests on unidirectional laminate.

From Fig. 11, by polynomial interpolation, it was obtained the coefficient β = 0.635 $(MPa)^{-3}$ for this type of lamina used in the study.

This constitutive relation can be implemented in USER_MAT user subroutine as it is described in [27]:

$$\tau_{12}^{(t+\Delta t)} = \frac{1+2\cdot\beta\cdot(\tau_{12}^t)^3\cdot(\gamma_{12}^t)^{-1}}{1+3\cdot\beta\cdot {G_{12}}^0\cdot(\tau_{12}^{(i)})^2}\cdot {G_{12}}^0\cdot\gamma_{12}^{t+\Delta t} \tag{2}$$

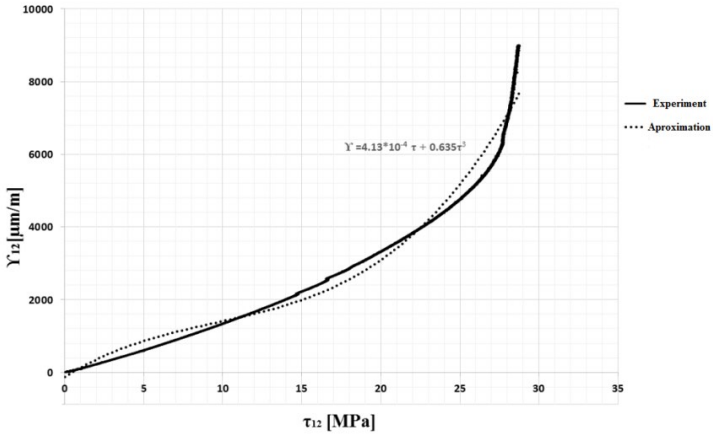

Fig. 11 Nonlinear shear–strain experimental curve

The orthotropic stress-strain constitutive relationship is given by equations (3) and (4), according to [28]:

$$\begin{bmatrix}\sigma_{11}^{t+\Delta t}\\ \sigma_{22}^{t+\Delta t}\\ \sigma_{33}^{t+\Delta t}\end{bmatrix}=\begin{bmatrix}E_{11}B(1-\vartheta_{23}\vartheta_{32}) & E_{22}B(\vartheta_{12}-\vartheta_{13}\vartheta_{32}) & E_{33}B(\vartheta_{13}-\vartheta_{12}\vartheta_{23})\\ E_{22}B(\vartheta_{12}-\vartheta_{13}\vartheta_{32}) & E_{22}B(1-\vartheta_{13}\vartheta_{31}) & E_{22}B(\vartheta_{32}-\vartheta_{12}\vartheta_{31})\\ E_{33}B(\vartheta_{13}-\vartheta_{12}\vartheta_{23}) & E_{22}B(\vartheta_{32}-\vartheta_{12}\vartheta_{31}) & E_{33}B(1-\vartheta_{12}\vartheta_{21})\end{bmatrix}\times\begin{bmatrix}\varepsilon_{11}^{t+\Delta t}\\ \varepsilon_{22}^{t+\Delta t}\\ \varepsilon_{33}^{t+\Delta t}\end{bmatrix} \tag{3}$$

$$\begin{bmatrix}\tau_{12}^{t+\Delta t}\\ \tau_{23}^{t+\Delta t}\\ \tau_{31}^{t+\Delta t}\end{bmatrix}=\begin{bmatrix}Rel.(6) & 0 & 0\\ 0 & G_{23} & 0\\ 0 & 0 & G_{31}\end{bmatrix}\times\begin{bmatrix}\gamma_{12}^{t+\Delta t}\\ \gamma_{23}^{t+\Delta t}\\ \gamma_{31}^{t+\Delta t}\end{bmatrix} \tag{4}$$

where:

$$B=\frac{1}{1-\vartheta_{12}\vartheta_{21}-\vartheta_{23}\vartheta_{32}-\vartheta_{13}\vartheta_{31}-2\cdot\vartheta_{21}\vartheta_{32}\vartheta_{13}} \tag{5}$$

$$\tau_{12}^{t+\Delta t}=\begin{cases}\dfrac{1+2\cdot\beta\cdot(\tau_{12}^{t})^{3}\cdot(\gamma_{12}^{t})^{-1}}{1+3\cdot\beta\cdot {G_{12}}^{0}\cdot(\tau_{12}^{t})^{2}}\cdot {G_{12}}^{0}\cdot\gamma_{12}^{(t+\Delta t)}, & FI=0\\ {G_{12}}^{t+\Delta t}\cdot\gamma_{12}^{t+\Delta t}, & FI\geq 1 \text{ and } {G_{12}}^{t+\Delta t}\cdot\gamma_{12}^{t+\Delta t}<\tau_{12}^{init}\\ \tau_{12}^{init}, & FI\geq 1 \text{ and } {G_{12}}^{t+\Delta t}\cdot\gamma_{12}^{t+\Delta t}\geq\tau_{12}^{init}\end{cases} \tag{6}$$

$$FI=max\,(FI_{1},\,FI_{2}) \tag{7}$$

In relation (6), G_{12}^{0} is the initial in-plane shear modulus which is reduced according to degradation rules specified in relation (11), once fiber compression-shear failure happened. The shear stress τ_{12}^{init} is a threshold used to avoid any over-estimation of the shear stress after any failure that can reduce the shear modulus G_{12}.

- Failure criteria and continuous degradation rules

The most dominant micro-failure modes for bearing joints are matrix compression and fiber shear-compression failures, so important attention is paid to them in this failure study. For the PDA of the laminated plate around the hole, Hashin [29] failure criteria is used and the failure indexes are calculated using relation (8) for matrix compression failure and relation (9) for fiber compression and matrix-fiber shear failure:

$$FI_1=\left[\left(\frac{\sigma_{22,\,\max}^{C}}{2\cdot\tau_{23}^{\max}}\right)^2-1\right]\cdot\frac{\sigma_2+\sigma_3}{\sigma_{22,\,\max}^{C}}+\frac{(\sigma_2+\sigma_3)^2}{4\cdot(\tau_{23}^{\max})^2}-\frac{\sigma_2\cdot\sigma_3}{(\tau_{23}^{\max})^2}+\left(\frac{\tau_{12}}{\tau_{12}^{\max}}\right)^2+\left(\frac{\tau_{13}}{\tau_{13}^{\max}}\right)^2+\left(\frac{\tau_{23}}{\tau_{23}^{\max}}\right)^2+\left(\frac{\sigma_1}{\sigma_{11,\,\max}^{T}}\right)^2 \quad (8)$$

$$FI_2=\left(\frac{\sigma_1}{\sigma_{11,\,\max}^{C}}\right)^2+\left(\frac{\tau_{12}}{\tau_{12}^{\max}}\right)^2+\left(\frac{\tau_{13}}{\tau_{13}^{\max}}\right)^2 \quad (9)$$

- Continuous degradation rules for elastic moduli

A strain-based degradation rule is proposed for reduction of E_{ii} (i=1…3) as described in [30]. The fiber or matrix failure initiate at a user-defined failure strain ε_{ii}^{init} and PDA stiffness reductions are performed using [30]:

$$E_{ii}^{t+\Delta t}=\begin{cases}E_{ii}^{0}\cdot\left(1-d_i\cdot\dfrac{\varepsilon_{ii}^{t+\Delta t}-\varepsilon_{ii}^{init}}{\Delta\varepsilon_{ii}}\right), & \varepsilon_{ii}^{init}\le\varepsilon_{ii}^{t+\Delta t}<\varepsilon_{ii}^{init}+\Delta\varepsilon_{ii}\\ E_{ii}^{0}\cdot(1-d_i)\dfrac{\varepsilon_{ii}^{init}+\Delta\varepsilon_{ii}}{\varepsilon_{ii}^{t+\Delta t}}, & \varepsilon_{ii}^{t+\Delta t}\ge\varepsilon_{ii}^{init}+\Delta\varepsilon_{ii}\end{cases} \quad (10)$$

where E_{ii}^{0} is the initial modulus of elasticity from Table 2 for lamina orthotropic directions, $\Delta\varepsilon_{ii}$ is a user-defined strain step to ensure a smooth reduction of the properties upon failure and d_i is the reduction factor. Initial failure strain and corresponding stress ε_{ii}^{init}, σ_{ii}^{init} are determined by simulation for FI = 1 according to relation (7).

- Continuous degradation rules for shear moduli

The in-plane shear modulus G_{12} is continuous reduced using the shear strain $\gamma_{ij}^{t+\Delta t}$ for FI > 1, according to [30]:

$$G_{ij}=G_{ij}^{0}\left(0.1+0.9\cdot\frac{\gamma_{ij}^{init}}{\gamma_{ij}^{t+\Delta t}}\right),\ i\neq j=1\ldots3 \quad (11)$$

The reduction parameters for E_{ii} (i=1… 3) are presented in Table 5 and obtained after several parameter tuning iterations.

Table 5. Degradation parameters for elastic moduli

Failure mode	d_i	$\Delta\varepsilon_{ii}$
Fiber shear-compression (i=1)	0.6	0.005
Matrix compression (i=2, 3)	0.8	0.005

- Poisson's coefficient reduction

In [30] a continuous reduction of the Poisson's ratio is proposed in order to comply with elastic stability of the orthotropic materials:

$$\vartheta_{12}=\vartheta_{12}^{0}\cdot\sqrt{\frac{E_1E_2^{0}}{E_2E_1^{0}}},\ \vartheta_{13}=\vartheta_{13}^{0}\cdot\sqrt{\frac{E_1E_3^{0}}{E_3E_1^{0}}},\ \vartheta_{23}=\vartheta_{23}^{0}\cdot\sqrt{\frac{E_2E_3^{0}}{E_3E_2^{0}}} \quad (12)$$

- Results and discussions

In order to better understand the nonlinear structural behavior and failure mechanisms in the joint, the load-displacement curves for the three geometric cases are presented in Fig. 12.

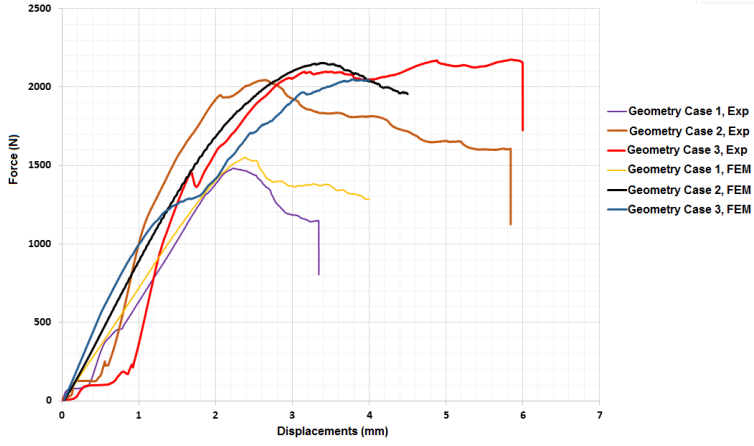

Fig. 12 Experimental and numerical load-displacement curves

Load-displacement curve for geometry case 1 is presented in Fig. 13 and simulation results regarding progressive failure around the hole in the laminated plate are presented in Figs. 14-16.

It is observed a nonlinear behavior due to friction between the plates at the beginning of force-displacements curve for test results, see Fig 13.

Increasing the applied tensile load up to approximately 155 N, the plates will not move relatively, due to static friction between them and the forces are transmitted only by friction.

Point A in Fig 13 represents the first damage initiation point, denoting the limit load of the joint and is located at the major deviation of the force-displacements curves from linear behavior.

At this point, the compression fibers damage first appears as an indicator of the bearing failure initiation, despite of shear damage to the fiber matrix, which is also recorded in Point A. As can be seen from Fig. 14, in 0^o plies the fibers damage are more predominant than matrix damage, while in 90^o plies the two micro level damages have almost the same spread out. In Fig. 13, point B represents the joint ultimate failure.

After point A, the damage accumulation causes a gradual reduction of joint stiffness and the characteristic curve becomes nonlinear.

From point A up to point B, the post failure stage is completely developed, where the residual stiffness is continuously reduced.

On this stage, the fiber compression, matrix compression and fiber-matrix shear damage are increasing at the bearing plane through the whole thickness of the laminate plate, as can be seen in Fig. 15.

Point C, in Fig. 13, represents the catastrophic final failure of the joint, when fiber compression, matrix compression and fiber-matrix shear damages start and propagate on approximately +/- 45^o from loading direction and extend to a large portion of the laminate plate on the bearing plane through free edge behind the hole of the laminate, as can easily be seen in Figs. 15 - 17.

A summary of the geometry effects on the progressive failure of the metal-composite hybrid joints is presented in Table 6 and Fig.18.

In Table 6, $F_{L.L}$ and $F_{U.L}$ represent the limit and ultimate forces of the joint to axial quasi-static tensile loading, corresponding to A and B points from the characteristic force-displacements curves, as discussed above.

From Table 6, it is clearly seen that bearing failure mode appears for all values of *w/d;*

the joint was designed in accordance with ASTM standard [17] to induce bearing failure.

In Fig. 18 it is presented the influence of the geometric parameter *w/d* on the joint ultimate failure load and it can be seen that the curve has an asymptotic value of 2200 N for the ultimate failure load.

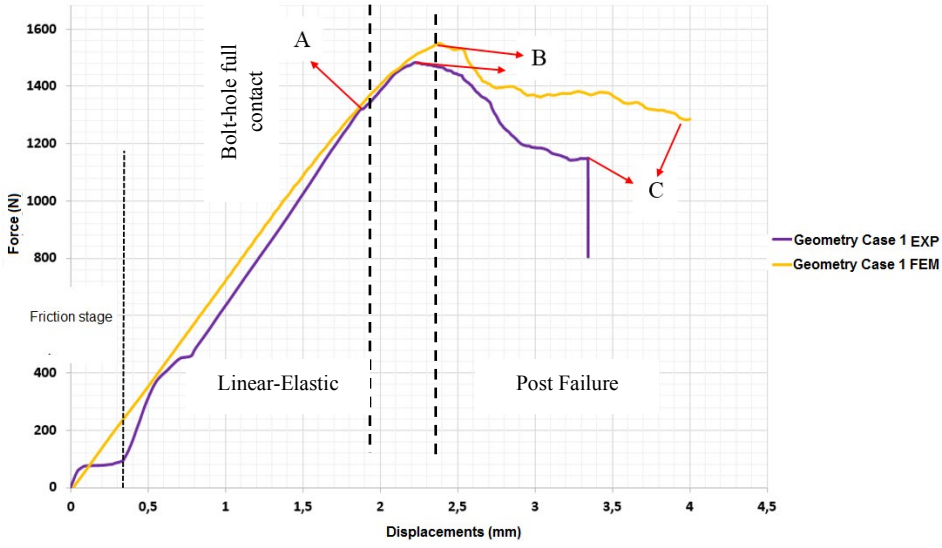

Fig. 13 Force-displacement curves. Geometry Case 1

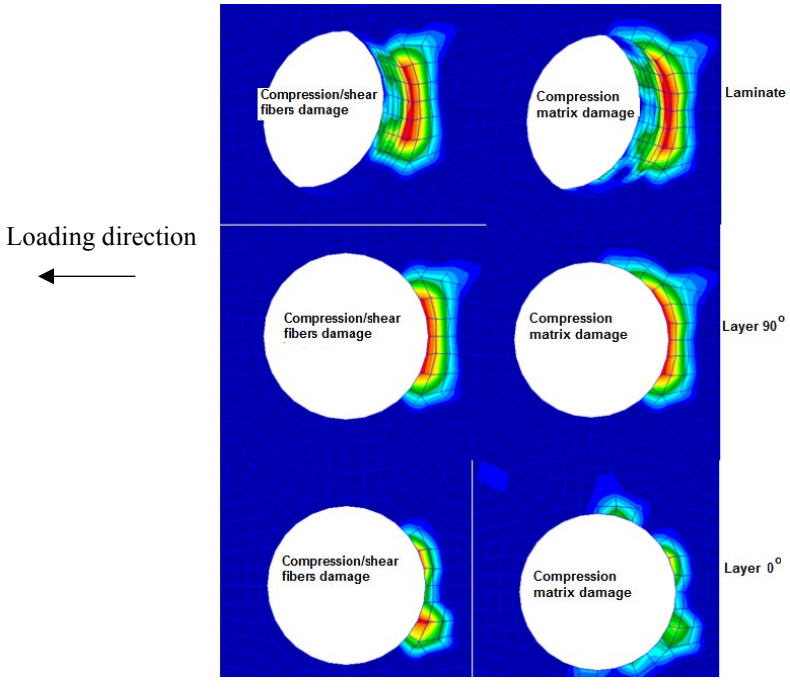

Fig. 14 Bearing damage initiation, point A. Geometry Case 1

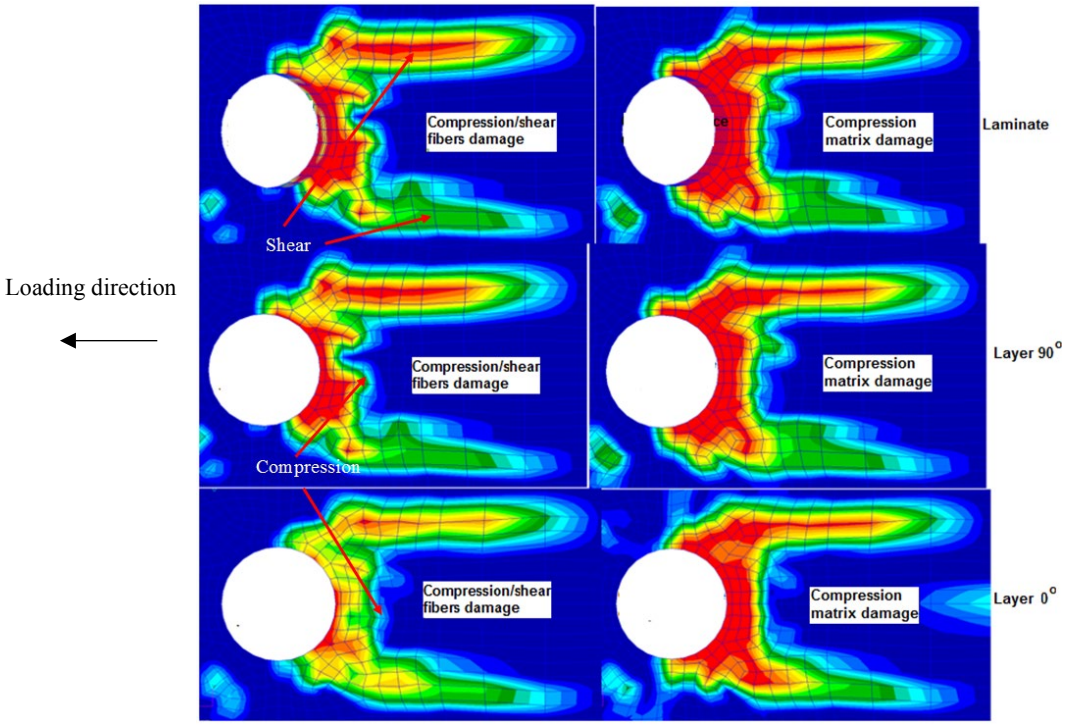

Fig. 15 Progressive damage, bearing/shear-out interaction, point B. Geometry Case 1

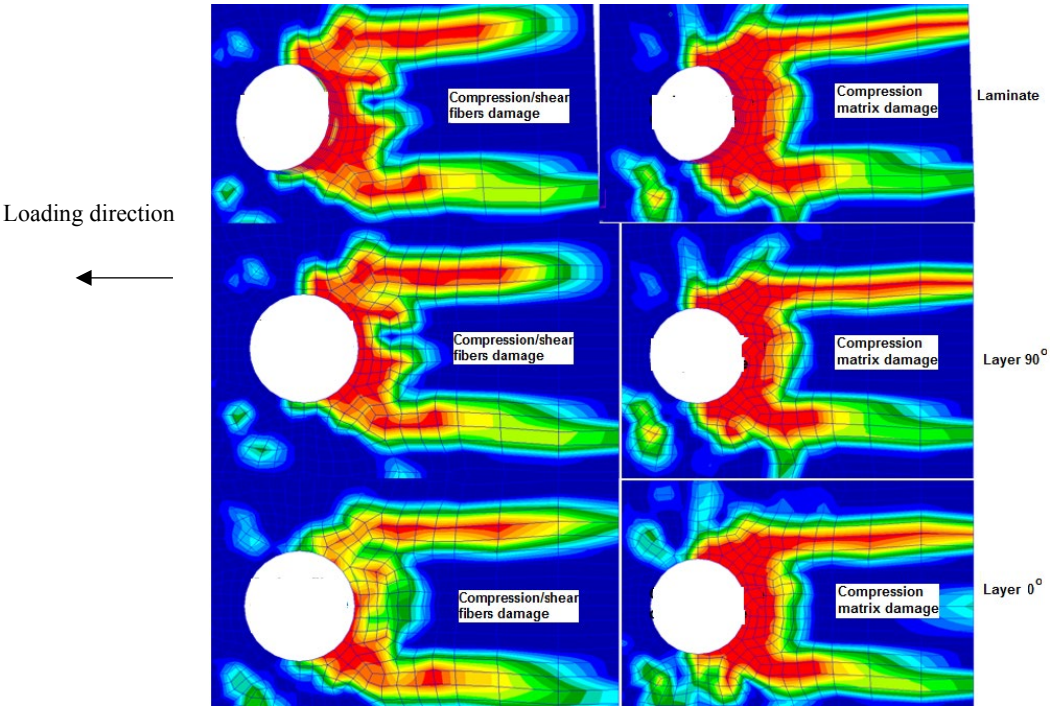

Fig. 16 Catastrophic failure, bearing/shear-out interaction, point C. Geometry Case 1

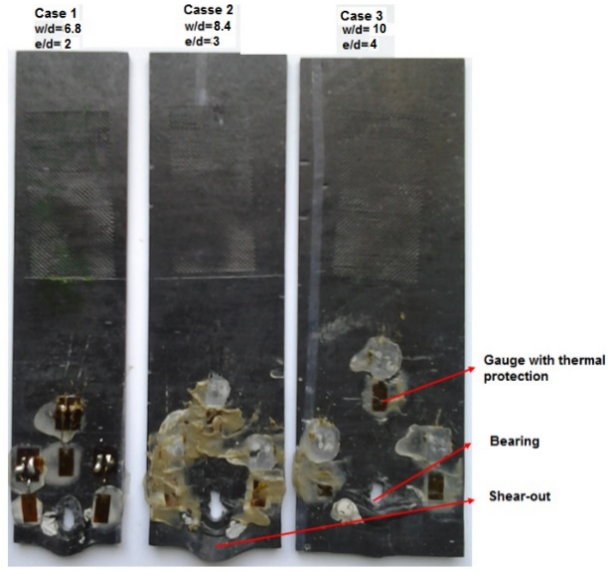

Fig. 17 The geometry influence on the joint failure modes

Table 6. Geometry effects on macroscopic failure modes of the joints

Geometry case	T [^{o}C]	Torque [Nm]	$F_{L.L}$ [N]	$F_{U.L}$ [N]	Failure mode		
			EXP	FEM	EXP	FEM	
w/d=6.8	50	0.5	1317.43	1376.65	1480.32	1548.94	Bearing/shear-out
w/d=8.4			1246.07	1225.65	2044.20	2043.94	Bearing/shear-out
w/d=10			1448.37	1500.03	2173.78	2151.84	Bearing

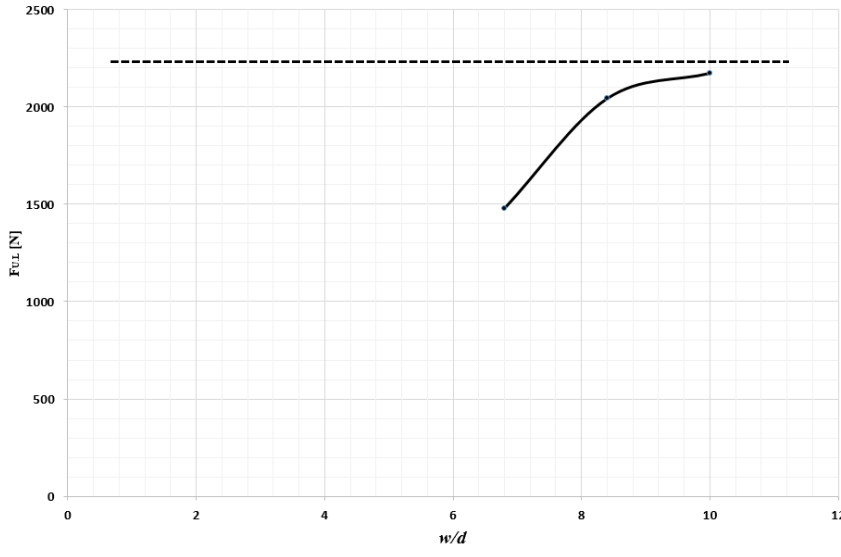

Fig. 18 The influence of geometric parameter *w/d* on joint ultimate failure load

4. CONCLUSIONS

In this paper, the plate geometry effects on the damage initiation and progressive failure of single-lap, single- bolt, hybrid metal-composite joints are investigated using both SHM (Structural Health Monitoring) experimental technique and simulations with finite element method (FEM). Regarding the first ply failure (FPF) and strength evaluations, a progressive damage analysis (PDA) including nonlinear shear behavior of the ply, Hashin failure criteria and strain-based continuous degradation rules was proposed. A 3D FEM model, which incorporates geometrical and contact full nonlinearities was developed in Patran, as preprocessor and Nastran, as explicit iterative solver. The PDA material model was implemented using a user-defined subroutine namely USER_MAT, using FOTRAN programming language.

The simulation results were in good agreement with the experiments in terms of surface strains, load-displacement behavior, FPF and ultimate failure loads, which denoted that the 3D FEM model including full nonlinearities and explicit solver are quite accurate and can predict the metal-composite joint's mechanical behavior on both linear-elastic and nonlinear elastic ranges, including the failure modes as bearing and shear-out. Regarding the geometry effects on the load-displacement curves, it can be seen from Fig. 8 that loading joint behavior released some interesting features at the beginning stage, due to friction between the plates. This friction stage is composed of two parts: static and dynamic friction. From these graphs it can be detected the friction load and, knowing the clamping force from torque level, therefore the friction coefficient between the plates can be calculated. Regarding the FPF and strength predictions, the SHM technique proved to be quite accurate in evaluating the damage initiation and accumulation until final failure.

In Fig. 18 it is presented the influence of the geometric parameter *w/d* on the joint ultimate failure load and it can be seen that the curve has an asymptotic value of 2200 N for the ultimate failure load.

ACKNOWLEDGEMENTS

Funding: This work was supported by the EU Structural Funding through "Be Antreprenor!" Project [grant number 51680/09.07.2019POCU/380/6/13-SMIS code: 124539], under the consideration of The "Politehnica" University of Bucharest.

REFERENCES

[1] Y. Xiao, T. Ishikawa, Bearing strength and failure behavior of bolted composite joints (part II: modeling and simulation), *Composites Science and Technology*, **65**(1), 1032–1043, 2005.

[2] J. L. Chaboche, Continuum damage mechanics: part I – General concepts; part II – damage growth, crack initiation and crack growth, *Journal of Applied Mechanics,* **55**, 59–72*,* 1988.

[3] F. K. Chang, K. Y. Chang, Post-failure analysis of bolted composite joints in tension or shear-out mode failure, *Journal of Composite Materials*, **21**, 809–33, 1987.

[4] L. B. Lessard, M. M. Shokrieh, Two-dimensional modeling of composite pinned-joint failure, *Journal of Composite Materials*, **29**, 671–97, 1995.

[5] C. L. Hung, F. K Chang, Bearing failure of bolted composite joints. Part II: model and verification, *Journal of Composite Materials*, **30**, 1359–400, 1996.

[6] S. J. Kim, J. S. Hwang, J. H. Kim, Progressive failure analysis of pin-loaded laminated composites using penalty finite element method, *AIAA Journal*, **36**(1), 75–80, 1998.

[7] P. P. Camanho, F. L. Matthews, A progressive damage model for mechanically fastened joints in composite laminates, *Journal of Composite Materials*, **3**3, 2248–80, 1999.

[8] B. Okutan, The effects of geometric parameters on the failure strength for pin-loaded multi-directional fiber-glass reinforced epoxy laminate, *Composites B. Eng*., **33**(8, 567–8), 2002.
[9] K. I. Tserpes, G. Labeas, P. Papanikos, Th. Kermanidis, Strength prediction of bolted joints in graphite/epoxy composite laminates, *Compos. B. Eng.*, **33** (7), 521–9, 2002.
[10] Á. Olmedo, C. Santiuste, On the prediction of bolted single-lap composite joints, *Composite Structures*, **94**(6), 2110–7, 2012.
[11] Z. Kapidz˘ic´, L. Nilsson, H. Ansell, Finite element modeling of mechanically fastened composite-aluminum joints in aircraft structures, *Composite Structures*, **109**(6), 198–210, 2014.
[12] A. K. Zerbst, G. Kuhlmann, C. Steenbock, et al., Progressive damage analysis of composite bolted joints with liquid shim layers using constant and continuous degradation models, *Composite Structures*, **92**(2), 189–200, 2010.
[13] G. Kolks, K. I. Tserpes, Efficient progressive damage modeling of hybrid composite/titanium bolted joints. *Composites A*, **56**(1), 51–63, 2014.
[14] B. Egan, M. A. McCarthy, R. M. Frizzell, P. J. Gray, C. T. McCarthy, Modelling bearing failure in countersunk composite joints under quasi-static loading using 3D explicit finite element analysis, *Composite Structures*, **108**, 963–977, 2014.
[15] Á. Olmedo, C. Santiuste, E. Barbero, An analytical model for the secondary bending prediction in single-lap composite bolted-joints. *Composite Structures*, **111**, 354–361, 2014.
[16] L. V. Awadhani, Dr. Anand K. Bewoor, Analytical and experimental investigation of effect of geometric parameters on the failure modes in a single lap single bolted metal to GFRP composite bolted joints subjected to axial tensile loading, *Proc. 4th ICAAMM*, 7345–7350, 2017.
[17] * * * ASTM D 5961, *Standard test method for bearing response of polymer matrix composite laminates*. American Society for Testing and Materials; 2007.
[18] * * * MMPDS-05, *Metallic Materials Properties development and Standardization*, Federal Aviation Administration, 2010
[19] * * * ASTM D 3039, *Standard Test Method for Tensile Properties of Polymer Matrix Composite Materials*, ASTM International, 2007.
[20] * * * ASTM D 5379, *Standard Test Method for Shear Propeties of Composite Materials by the V-Notched Beam Method*, ASTM International, 2008.
[21] * * * ASTM D 3410, *Standard Test Method for Compressive Properties of Polymer Matrix Composite Materials*, ASTM International, 2007.
[22] M. A. McCarthy, C. T. McCarthy, V. P. Lawlor, W. F. Stanley, Three-dimensional finite element analysis of single-bolt, single-lap composite bolted joints: part I - model development and validation, *Composite Structures*, **71**, 140-158, 2004.
[23] H. Lamb, On Waves in an Elastic Plate, *Proc. of the Royal Society, Mathematical, Physical and Engineering Sciences*, **93**, 114 – 128, 1917.
[24] V. Giurgiutiu, J. Bao, Embedded Ultrasonic Structural Radar with Piezoelectric Wafer Active Sensors for the NDE of Thin-Wall Structures, *Proc. ASME International Mechanical Engineering Congress*, New Orleans, USA, 2002.
[25] * * * http://www.steminc.com/piezo/PZ_property.asp.
[26] H. T. Hahn, S. W. Tsai, Nonlinear elastic behavior of unidirectional composite laminates, *Journal of Composite Materials,* **7**(1), 102–18, 1973.
[27] A. Du, Y. Liu, H. Xin, Y. Zuo. Progressive damage analysis of PFRP double-lap bolted joints using explicit finite element method, *Composite Structures* **152**, 860–869*,* 2016.
[28] Z. Hashin, Failure criteria for unidirectional fiber composites, *Journal of Applied Mechanics,* **80**(47)*,* 329–342, 1973.
[29] Y. Zhou, H. Yazdani-Nezhad, M. A. Mccarthy, et al. A study of intra-laminar damage in double-lap, multi-bolt, composite joints with variable clearance using continuum damage mechanics, *Composite Structures,* **116** (9), 441–52, 2014.
[30] R. M. O'Higgins, *An experimental and numerical study of damage initiation and growth in high strength glass and carbon fibre-reinforced composite materials,* doctoral diss., University of Limerick, College of Engineering, Limerick, 2007.